Penerbit Akademia Baru

Journal of Advanced Research Design

Journal homepage:
https://akademiabaru.com/submit/index.php/ard
ISSN: 2289-7984

Improved Colour Visualization in Pap Smear Images Based on HSV Channel Analysis

Khalis Danial Nukman Khiruddin[1] , Wan Azani Mustafa[1,2,*], Khairul Shakir Ab Rahman[3], Hiam Alquran[4], Syahrul Junaini[5]

[1] Faculty of Electrical Engineering & Technology, Universiti Malaysia Perlis, Pauh Putra Campus, 02600 Arau, Perlis, Malaysia
[2] Advanced Computing (AdvComp), Centre of Excellence (CoE), Universiti Malaysia Perlis (UniMAP), Campus Pauh Putra, 02600 Arau, Perlis, Malaysia
[3] Department of Pathology, Hospital Tuanku Fauziah, Jalan Tun Abd Razak Kangar 01000, Perlis, Malaysia
[4] Biomedical Systems and Medical Informatics Engineering, Yarmouk University, 21163 Irbid, Jordan
[5] Faculty of Computer Science & Information Technology, Universiti Malaysia Sarawak, 94300 Kota Samarahan, Sarawak, Malaysia

ARTICLE INFO

Article history:
Received 6 January 2025
Received in revised form 28 February 2025
Accepted 10 March 2025
Available online 28 March 2025

Keywords:
Pap smear; cervical cell; nucleus; contrast enhancement; denoise

ABSTRACT

Cervical cancer is caused by abnormal cell growth in the female cervix. It is among the most well-known causes of women's deaths globally. Early detection of cervical cancer can reduce the mortality rate and increase the chance of survival. One of the most critical components of the auto-detection system is image pre-processing. The main factors that could influence the accuracy of the diagnosis are the Pap smear image quality and contrast. Therefore, this paper aims to analyse various approaches to ensure smooth segmentation and determine which pre-processing techniques are best for a nucleus auto-detection system. Two hundred images were used as input from the Herlev dataset. There are two pre-processing stages: noise removal and contrast enhancement. To preserve the colour, only the colour images' brightness (V) channel will go through the pre-processing. Without noise, the anticipated resultant image depicts only the object (nuclei and cytoplasm) and background. Results show that the median filter produces the best result regarding smoothening and debris removal in visual analysis. At the same time, Pairing Adaptive Gamma and Clipping Histogram Equalisation (PAGCHE) method produces the best brightness and contrast improvement results based on visual and quantitative analysis. The results were compared with anisotropic diffusion, Non-Local Haar (NLH), and bilateral filters in the denoise stage and histogram equalisation, contrast stretching, and Contrast Limited Adaptive Histogram Equalisation (CLAHE) for the contrast enhancement stage. The performance was evaluated based on mean, absolute mean brightness error (AMBE), standard deviation (STD), structural similarity index metric (SSIM), peak signal-to-noise ratio (PSNR), and entropy. The average PAGCHE shows the highest Mean and AMBE values at 148.07 and 21.96, respectively, while the STD value is the second highest compared to other methods at 60.4. The median filter produces the lowest SSIM score and low PSNR scores compared to the others but relatively high values at 0.71 and 15.38, respectively, with an entropy of 7.30, indicating a good noise removal ability that can be observed in visual analysis.

* *Corresponding author.*
E-mail address: wanazani@unimap.edu.my

https://doi.org/10.37934/ard.126.1.99120

1. Introduction

In the cells of the cervix, cervical cancer originates from the lower portion of the uterus that is anatomically connected to the vagina. It occurs when the cells of the cervix increase abnormally. Nadzirah *et al.,* [1] stated that this will spread to organs and tissues surrounding the cervix, including the lungs and liver. As per the National Cancer Institute's data in [2,3], cervical cancer ranks as the fourth most prevalent malignancy among women globally. An estimated 604,000 new cases of cervical cancer and 342,000 deaths occurred globally in 2020 [2,4]. Mustafa *et al.,* [5,6] highlighted in their papers that cervical cancer is a common form of the disease that likely every woman will eventually develop; furthermore, it is associated with a high mortality rate. This is due to the fact that early detection of cervical cancer is difficult to achieve globally, and by the time it is detected, the disease has progressed significantly.

Established during the 1940s by Georgios Papanikolaou, the Papanicolaou test is also known as the Pap test or Pap smear. It has exfoliating cells from the improvement range of the cervix, which enables microscopic analysis of these cells to detect precancerous or cancerous cells [7]. Patel *et al.,* [8] stated a brief procedure of the pap smear test where a speculum is used to examine the cervix while the patient is in the lithotomy position. Ayre's spatula's smaller end is inserted through the external os using a speculum, and it is rotated 360 degrees to scrape the squamocolumnar junction. The traditional method of cervical cancer screening is based on the Pap smear test. However, this method has several limitations, including low sensitivity and specificity, which can lead to false-negative [9] or false-positive results [10].

By enhancing the quality of Pap smear images, image enhancement techniques can aid in the detection of cervical cancer [11]. The microscopic image sample is susceptible to artefacts, blurring, noise, shadow, and lighting issues [12]. A microbiologist can only make a diagnosis based on microscopic observations. As a result, even with experienced hands, it is time-consuming, and inaccurate results are still possible [13]. Low-quality visual images are difficult to perceive, as are image processing and computer vision applications [14-16]. Therefore, image quality should be enhanced before they are used to create images that are highly suitable for human visual perception and simple for machines to evaluate. This will also enhance computer vision applications [16-18]. Image enhancement techniques can improve images' contrast, brightness, and sharpness, making it easier to identify abnormal cells [19]. Accurate diagnosis data is essential for helping a physician assess a patient's condition. By applying image enhancement techniques, it is possible to decrease the number of false-positive or false-negative results and increase the accuracy of cervical cancer screening.

There are several classical filter methods for image denoising, such as the median filter [20], mean filter [21], Gaussian filter [22], and Fourier transform [23]. Another widely used method is the Non-Local Means (NLM) [24], which improves image quality by looking for relevant information within the same image. Furthermore, several cutting-edge approaches have been employed, each producing a distinct denoising effect. Jaspin and Suganthi, for instance, propose a new Adaptive Switching Modified Decision-Based Unsymmetric Trimmed Median Filter (ASMDBUTMF) for noise removal in grey-level MR images impacted by black and white pixel noise [25]. Bhawna *et al.,* [26] introduced a new hybrid method that employs a cross bilateral filter (CBF) to prevent smoothing the edges prior to performing several mathematical operations. These detail images are then processed further with a rolling guidance filter (RGF), which removes small-scale structures while refining edges to preserve immense detail image structures. In the Volkan Göreke method, the Wiener filter is modified using the Finite impulse response (FIR) filter embedded in the standard Wiener algorithm. The Atom Search Optimization (ASO) optimisation algorithm was used to design the FIR filter. The optimisation matrix

corresponding to the FIR filter coefficients is used to calculate the optimal local mean and optimum local variance values, which are then transferred to the standard Wiener filter layer as parameter inputs [27]. Divya *et al.,* [28] study a hybrid approach for designing a denoising filter for medical images that integrates a new guided decimation box filter (GDBF) with a hybrid cuckoo particle swarm optimization (HCPSO) algorithm. The suggested method by Rajanbir *et al.,* [29] begins with a threshold and then denoises the image using a combination of linear, non-linear, and probabilistic techniques. Furthermore, a universal add-on is presented to improve the quality by brushing out fine details from the restored image using edge detection and smoothening techniques. To eliminate high-density impulsive noise, Nikhil *et al.,* [30] proposed an adaptive weighted min-mid-max value-based filter.

Numerous studies on colour and contrast adjustment methods have been executed. Image enhancement is essential in image processing because it enhances valuable information [31] while reducing unnecessary information in an image [32]. Since most picture improvement methods are based on basic concepts, image enhancement is highly appealing [17]. In recent decades, image enhancement based on contrast and luminosity correction has been focused on [11-13,19,33-35]. Several cutting-edge methods have been reported in recent years. Bilal Bataineh, [16] for instance, suggested a unique method for correcting colour images using the benefits of non-linear function in grey transformation and histogram equalisation techniques. Karishma Rao [36] introduced using the Just Noticeable Distortion (JND) model and multiple layers of Contrast Limited Adaptive Histogram Equalisation (CLAHE), a compelling image enhancement method for improving the luminosity and contrast of colour retinal fundus images. Saroj [37] proposed a new technique for this purpose that combines principal component analysis (PCA), multi-scale switching morphological operator (MSMO), and CLAHE methods in a novel sequence. Based on a fuzzy approach, Mousania *et al.,* [38] proposed a new composition of CLAHE and brightness-preserving dynamic fuzzy histogram equalisation techniques with appropriate weights according to the histogram situation.

2. Methodology

2.1 Image Acquisition

The 917 sample images were collected from the Herlev database (Herlev University Hospital, Denmark). The database was obtained from/developed by NiSIS (EU coordination action, contract 13569), a Nature-inspired Smart Information System, with particular significance for the Nature-Inspired Data Technology focus group. It is thus accessible (http://fuzzy.iau.dtu.dk/download /smear2005) on the World Wide Web.

2.2 Noise Filtering

Noise filtering stages evaluate three types of classical denoise filters, which are the median filter, anisotropic diffusion filter [39], bilateral filter [40], and one state-of-art filter, the Non-Local Haar (NLH) filter proposed by [41].

2.2.1 Median filtering

Median filters are useful in reducing random noise, especially when the noise amplitude probability density has large tails and periodic patterns [42]. The median filtering process involves sliding a window over the image and replacing each pixel with the median value of the pixels within the window. This method is particularly effective for removing salt-and-pepper noise while

preserving edges, as it uses the median as the maximum likelihood estimator of location in the presence of Laplacian noise distribution. In relatively uniform areas, the median filter successfully estimates the grey-level value, with a notable advantage in handling long-tailed noise. When crossing edges, the filter allows one side of the edge to dominate, ensuring that the edge remains sharp and unblurred. While the median filter is excellent for eliminating impulse noise, it may be less effective against Gaussian noise. Additionally, using a large window size can blur fine details in the image. In this study, a window size of 20x20 pixels was selected to balance noise reduction and the preservation of important image features. The "Replicate" method was employed for border handling, which replicates the nearest border pixel value when the filtering window overlaps the edge of the image. This approach minimises artefacts and preserves the integrity of the edge regions. The implementation steps are shown in Algorithm 1 with the parameter set in Table 1.

Algorithm 1: Median filtering algorithm

Input :*image, windowSize*
Output :*filteredImage*
Initialize *filteredImage* with the same dimensions as image
Define *halfWindowSize* as floor(*windowSize*/2)
for each pixel (*i, j*) in image:
    window ← []
    for k **from** -*halfWindowSize* **to** *halfWindowSize* **do**
        for *l* from -*halfWindowSize* to *halfWindowSize* **do**
            if (*i* + *k*) is within the height bounds of image AND (*j* + *l*) is within the width bounds of image **then**
                append image[i + k][j + l] to *window*
        sort *window*
        filteredImage[i][j] ← median(*window*)
return *filteredImage*

Table 1
Median filter parameters

Parameter	Value
Window Size	20x20
Border Handling	Replicate

2.2.2 Anisotropic diffusion filtering

Anisotropic diffusion, or Perona–Malik diffusion, is a fundamental technique in image processing that adapts its behaviour based on local content, unlike isotropic diffusion, which uniformly smooths an image. By employing a threshold function, it selectively diffuses across homogeneous regions while preserving critical features such as edges and lines. This makes it particularly useful for denoising images without sacrificing essential details. The ability to adapt to the image's structure enhances visual quality and preserves crucial information. However, anisotropic diffusion is computationally more complex than simpler filters like the median filter and requires careful tuning of parameters such as the gradient threshold and number of iterations for optimal performance. The implementation steps are shown in Algorithm 2 with the parameter set in Table 2.

Algorithm 2: Anisotropic diffusion filtering

Input : *image, numIterations, kappa, gamma*
Output : *filteredImage*
Initialize *filteredImage* with the input image
for t from 1 to numIterations **do**
    Compute gradients in four cardinal directions
    Compute diffusion coefficients
    Update the image using the diffusion equation
return *filteredImage*

The mathematical representation of anisotropic diffusion filtering is based on the partial differential equation (PDE) for image intensity evolution over time. The anisotropic diffusion process is described by the PDE *expression* in Eq. (1):

$$\frac{\partial I}{\partial t} = \nabla \cdot (c(x,y,t)\nabla I) \tag{1}$$

Where:

- $I(x,y,t)$: The image intensity at position (x,y) and time t.
- ∇I : The gradient of the image (rate of intensity change).
- $\nabla \cdot$: The divergence operator, which measures the net flux of the vector field $c(x,y,t)\nabla I$.
- $c(x,y,t)$: The diffusion coefficient, which controls the rate of diffusion and is a function of the gradient magnitude.

The diffusion coefficient $c(x,y,t)$ is designed to vary based on the gradient magnitude to preserve edges. The most common form is represented as shown in Eq. (2), where $\|\nabla I\|$ is the gradient magnitude and k is the edge threshold parameter.

$$c(\|\nabla I\|) = exp\left(-\left(\frac{\|\nabla I\|}{k}\right)^2\right) \tag{2}$$

Table 2
Anisotropic diffusion filter parameters

Parameter	Value
numIterations	20
kappa	20
gamma	0.2
Diffusion Coefficient Function	Exponential

2.2.3 Bilateral filtering

Bilateral filtering, a non-linear edge-preserving technique, is fundamental in image denoising. Unlike linear filters that uniformly smooth pixel values, bilateral filtering considers both spatial distance and pixel intensity similarity. By incorporating a weighted average of these factors, it selectively smooths homogeneous regions while preserving critical edges. Key parameters, including diameter, colour space, and coordinate space, are crucial for balancing noise reduction and edge preservation. One challenge is selecting appropriate parameters, such as spatial and intensity sigma values, as incorrect choices can lead to suboptimal denoising or loss of details. Additionally, the

bilateral filter's computational cost is higher than simple linear filters, which is a consideration for large images. The filtered pixel value at location (x, y) is calculated as follows in Eq. (3):

$$I_{filtered}(x,y), = \frac{1}{W_p}\sum_{u,v} I(u,v) \cdot G_{\sigma_s}(\|(x,y)-(u,v)\|) \cdot G_{\sigma_r}(|I(x,y)-I(u,v)|) \quad (3)$$

Where:

- $I_{filtered}(x,y)$ is the filtered pixel value at location (x,y).
- $I(u,v)$ is the intensity value of the pixel at location (u,v).
- $G_{\sigma_s}(\|(x,y)-(u,v)\|)$ is the spatial Gaussian function that measures the spatial distance between the pixels (x,y) and (u,v).
- $G_{\sigma_r}(|I(x,y)-I(u,v)|)$ is the range Gaussian function that measures the intensity difference between the pixels (x,y) and (u,v).
- W_p is a normalization factor to ensure the weights sum to 1.

The spatial Gaussian function is given by Eq. (4) below where r is the spatial distance $\|(x,y)-(u,v)\|$, and σ_s controls the extent of the spatial influence (larger values lead to a wider range of spatial smoothing).

$$G_{\sigma_s}(r) = exp\left(-\frac{r^2}{2\sigma_s^2}\right) \quad (4)$$

whereas the range Gaussian function can be expressed as Eq. (5) shown below where d is the intensity difference $|I(x,y)-I(u,v)|$, and σ_r controls the extent of the intensity-based smoothing (larger values allow more intensity difference to contribute to smoothing). The parameters are set and is shown in Table 3.

$$G_{\sigma_r}(d) = exp\left(-\frac{d^2}{2\sigma_r^2}\right) \quad (5)$$

Table 3
Bilateral filter parameters

Parameter	Value
Spatial Sigma, σ_s	10
Color Sigma, σ_r	30
Kernel Size	9x9

2.2.4 Non-local Haar filtering

The NLM method of denoising aims to restore image quality by selectively averaging pixel values. Unlike traditional "local mean" filters that consider a group of neighbouring pixels, non-local mean filters take into account all pixels in the image. The main framework of this method consists of three steps: searching for non-local similar pixels, as shown in Figure 1, noise level estimation, and a two-stage denoising framework, as shown in Figure 2 and described in Algorithm 3.

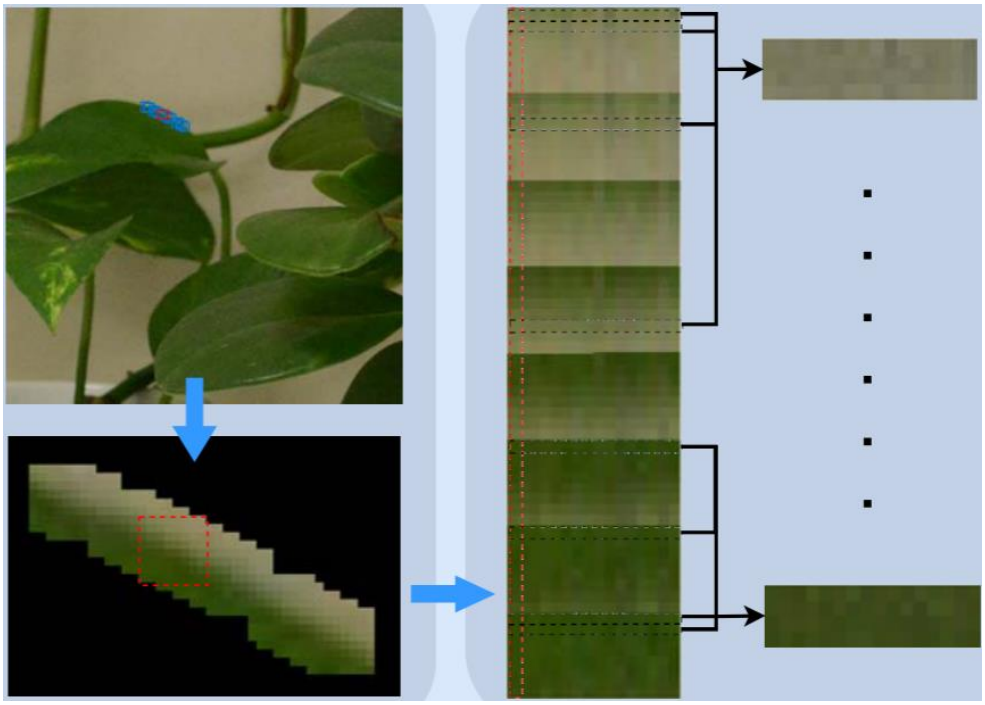

(a) (b)

Fig. 1. Non-local similar patches [41]

Based on Figure 1, from each image patch (e.g., the patch in the red box), its non-local similar patches (e.g., the patches in blue boxes) are searched. Then, similar patches are transformed into columns of vectors, as shown in (b). For each row of pixels, their non-local similar pixels (e.g., the rows of pixels in black boxes) are searched within the previously searched similar patches in (a). Next, the second step is to estimate the noise level introduced to the pixel-level NSS prior to achieving an accurate and fast estimation of noise levels. Standard deviation, σ, is computed using the formula shown in Eq. (6):

$$\sigma_l = \frac{1}{n(q-1)} \sum_{t=2}^{q} \sum_{i=1}^{n} \sqrt{\frac{1}{m} (d_l^{ii_t})^2}. \quad (6)$$

To make the noise estimation method more robust towards texture and structures, the author extended the noise level estimation from a local region to a global one. To do so, local noise levels estimated for all the noisy pixel matrices in the image, and simply set the global noise level as shown in Eq. (7):

$$\sigma_g = \frac{1}{N} \sum_{l=1}^{N} \sigma_l \quad (7)$$

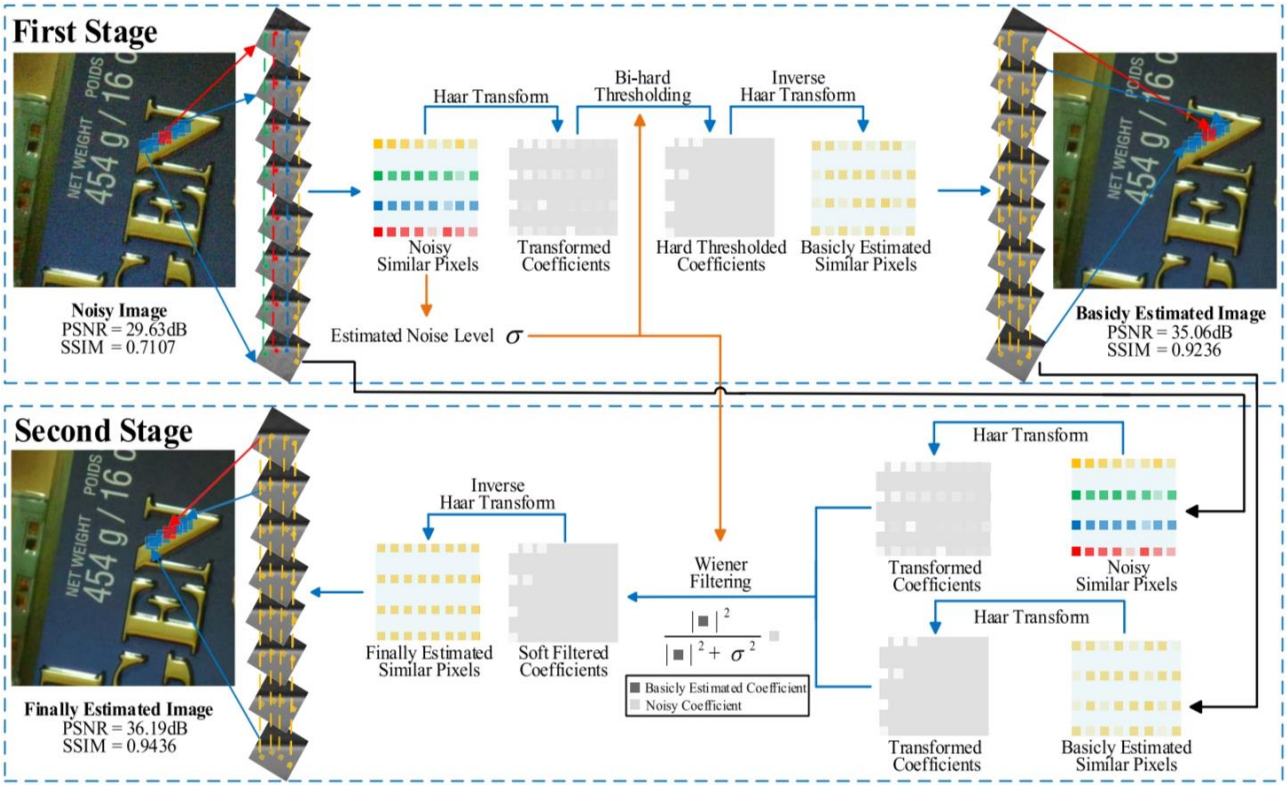

Fig. 2. Two-stage denoising framework

Algorithm 3: Two stages framework of non-local Haar filtering

Stage 1: Initial Denoising
1: Extract non-local similar
2: For each patch:
3: Identify similar pixels within the patch
4: Average similar pixels to reduce noise while preserving structure
5: Estimate noise level for each group of similar pixels
7: Apply Haar Transform to the matrix of similar pixels
8: Perform bi-hard thresholding to filter out noise
9: Apply inverse Haar Transform to obtain preliminary denoised image
Stage 2: Refined Denoising
10: Apply Haar Transform to the similar pixel matrices of both the original noisy image and the preliminary denoised image
11: Process the transformed coefficient matrices using Wiener filtering
12: Apply inverse Haar Transform to reconstruct the estimated similar pixel matrices
13: Combine the matrices to form the final denoised image

The NLH filter enhances the detection of weak particles by using a particle probability image, which is particularly useful in cell imaging where small particles are of interest. It achieves a higher PSNR in denoised images, indicating better noise reduction and feature preservation compared to other methods. Pap smear images contain fine cellular structures that require careful denoising. The two-stage framework of the NLM filter allows for accurate noise estimation and targeted denoising, which is especially beneficial in medical imaging where preserving fine details is crucial for accurate analysis and diagnosis. However, the computational demands of the NLH filter are significant, making it less suitable for real-time applications. Additionally, the performance of the filter can be sensitive to parameter choice, requiring careful tuning for optimal results.

2.3 Contrast Enhancement

2.3.1 Contrast limited adaptive histogram equalisation (CLAHE)

CLAHE is a sophisticated image processing technique that enhances contrast within an image. Unlike general histogram equalisation, which operates on the entire image, CLAHE works on small regions known as tiles. The adaptive nature of this method allows for contrast enhancement to be calculated individually for each tile, redistributing pixel values according to the local histogram. To avoid boundary artifacts, neighbouring tiles are seamlessly merged. Additionally, the technique limits contrast enhancement in homogeneous areas to prevent the amplification of noise present in the image. For the problem at hand, adaptive histogram equalisation is employed, demonstrating its utility in improving image quality while mitigating noise. This method remains relevant and is frequently employed by contemporary researchers [43-45], reflecting its enduring value in the field of image processing.

In this process, the image is divided into small blocks called tiles (e.g., tile size 8x8). The histogram of each tile is equalised independently. If noise is present, it may be amplified. To avoid this, contrast limiting is applied. If any histogram bins exceed the specified contrast limit, those pixels are clipped and distributed uniformly to other bins before applying histogram equalisation. After equalisation, bilinear interpolation is applied to remove artifacts at the tile borders.

2.3.2 Pairing adaptive gamma with clipping histogram equalisation (PAGCHE)

A novel method proposed by Bataineh [16] for colour image correction, based on the advantages of non-linear functions in grey transformation and histogram equalisation techniques, is adapted in this work. The process of the method is shown in Figure 3. Firstly, the original red, green, and blue (RGB) image is converted into the HSV colour space, and the V channel is used for enhancement. An adaptive gamma generator is proposed to adaptively calculate gamma parameters according to dark, medium, or bright image conditions. The computed gamma parameters are used to propose a cumulative distribution function that produces an optimised curve for illumination values. Next, a second modified equalisation is performed to evenly correct the offset of the illumination curve values based on the equal probability of the available values only. Finally, the processed V channel replaces the original V channel, and the new HSV model is converted back to the RGB colour space.

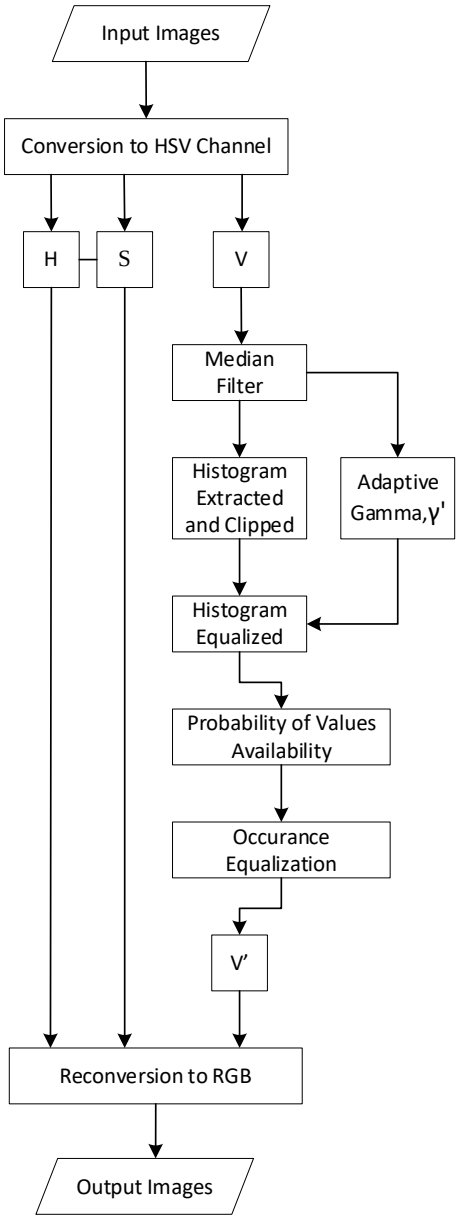

Fig. 3. Pairing adaptive gamma with clipping histogram equalisation

2.3.3 Histogram equalisation

Histogram equalisation is a fundamental technique in the realm of image processing. When an image predominantly occupies a narrow range of intensity values, it tends to appear flat and lacks visual dynamism. Histogram equalisation steps in to rectify this limitation. Hence, the primary objective is to enhance the contrast within an image by redistributing the intensity values across the entire spectrum. Figure 4 shows the flow process of the histogram equalisation used in this study.

This method is applied by distributing the greyscale value (GV) levels. In general, this is done by increasing the lower limit of the range of colours to the darkest point and decreasing the upper limit of the range of colours to the brightest point. The following formula was used to calculate the GV using the histogram equalisation equation shown in Eq. (8) below,

$$S = \sum_{j=0}^{k} \frac{n_j}{n}, \quad (8)$$

where n is the number of data, k is the range of GV, and S is the number of data on the GV.

By judiciously adjusting the intensity distribution, this method achieves a twofold purpose: first, it boosts the global contrast of numerous images, and second, it ensures that the full range of intensities is effectively utilised. Consequently, regions with initially lower local contrast experience an elevation in their contrast levels. Notably, this technique proves particularly valuable in scenarios where both the background and foreground exhibit either bright or dark characteristics.

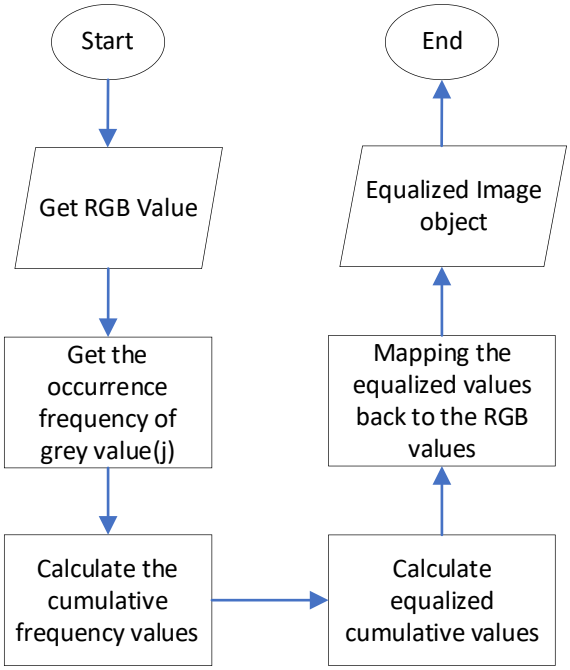

Fig. 4. Histogram equalisation

2.3.4 Contrast stretching

Contrast stretching, also known as normalisation, is a simple image enhancement technique. The quality of an image is enhanced by stretching the range of intensity values. To perform the stretching, upper and lower-pixel value limits must be specified over which the image is to be normalised. Then, each pixel PP is scaled using the following Eq. (9):

$$P_{out} = (P_{in} - c)\left(\frac{b-a}{d-c}\right) + a, \quad (9)$$

where a is the lower limit and b is the upper limit. Meanwhile, c and d are the existing lowest and highest pixel values, respectively. P is the pixel value.

3. Results

3.1 Qualitative Analysis

This research consists of two main image processing stages: a denoising stage that evaluates three types of classical denoising filters—the median filter, anisotropic diffusion filter [39], and

bilateral filter [40] —along with one state-of-the-art filter, the NLH filter proposed by [41]. The second stage is the contrast enhancement stage. A state-of-the-art low light contrast enhancement method offered by Bataineh [16] was used to compare with three other classical contrast enhancement methods: CLAHE [46], contrast stretching, and histogram equalisation [47]. To preserve the colour, all the filters and techniques are applied to the image's brightness (V channel of the HSV channels), while maintaining the hue (H) and saturation (S) channels.

This section employs two types of analysis, visual and quantitative, to assess the approaches. In visual testing, the subjective perception of human eyesight is used to quantify image quality. Humans have a decent understanding of image quality because these investigations are limited to visually evaluating image quality. The methods are applied to images from the previously described datasets. Figures 6–21 feature the selections and presentations of the four most intriguing situations. Figure 6(a) depicts the result of applying an anisotropic diffusion filter to the filtered image of Image 1 from Figure 5. Figures 6(b-e) show the results of the denoised image from Figure 6(a) after using four different contrast enhancement methods. The filtering process is repeated in Figures 7-9(a) for Image 1 with other denoising filters within the same contrast enhancement methods in Figures 7-9(b-e). Lastly, the process is repeated for different image datasets according to Figure 5 in Figures 10-21.

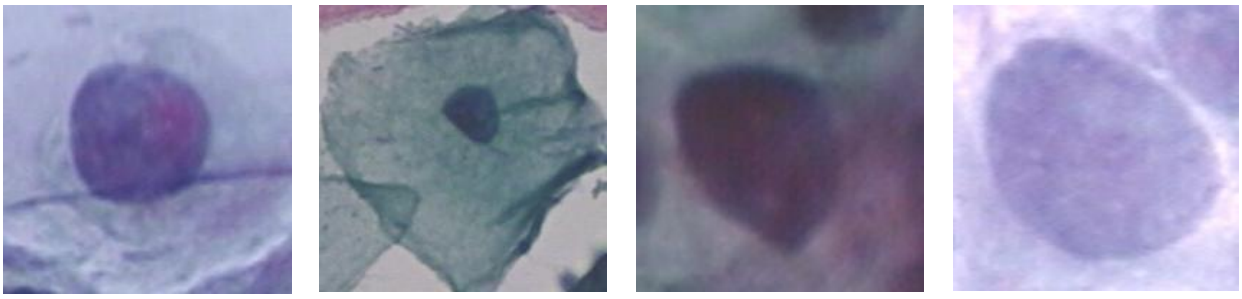

(a) Severe Dysplasia (b) Normal Intermediate (c) Moderate Dysplasia (d) Carcinoma in Situ

Fig. 5. Selected original images from four cervical cell classes

The results reveal that, depending on the approach employed, all of the selected images are visually enhanced differently. The effect of the denoise filter can be seen clearly in column (a) of Figures 6-21. In terms of smoothing the noise in the intracellular fluid and the nucleus, applying bilateral and median filters to Image 1 yielded good results in Figures 7(a) and 8(a). However, compared to the median filter, the bilateral filter fails to preserve the nucleus's edge, as evidenced by the blurring effect around the nucleus's edges in Figure 7(a). Additionally, compared to the other filters, the median filter produces the best results for removing the thin dark line. The median filter is also more effective than the bilateral filter in reducing the shadow effect on the cytoplasm and noise presence in Image 2, as seen in Figures 11(a) and 12(a). The NLH filter offered the best results in terms of detail preservation for Images 1 and 2. The anisotropic diffusion filter appears to have an insignificant effect compared to the others. In general, using a denoise filter improves all images over the originals, which is to be expected.

Visually comparing the results of the contrast enhancement methods applied to the images provides insight into the ability of the methods to differentiate the object of interest from the background. Based on Figures 6-9(b-e), applying CLAHE in column (b) to the denoised images does not significantly increase contrast. Conversely, PAGCHE, histogram equalisation, and contrast stretching methods produce enhanced images with relatively high contrast. However, in Images 1 and 2 in Figures 6-13(d), it can be observed that histogram equalisation fails to differentiate between the nucleus and cytoplasm. PAGCHE and contrast stretching, applied to all images in columns (c) and (e), can visually distinguish between the nucleus and background. However, the combination of the

NLH filter and contrast stretching produces low-light images in column (e) of Figures 9, 13, and 17. Applying all of the contrast enhancement methods to Image 4 in Figures 18-21 produced good overall results. It is important to note that the right combination of denoise filter and contrast enhancement can produce good results, even if one method alone does not. For example, when applying histogram equalisation to Image 2 in Figures 10-13 column (d), it can be observed that Figure 12 produces a good contrast distribution compared to the others. This indicates that applying histogram equalisation to the median-filtered image produces better results compared to other denoise filters.

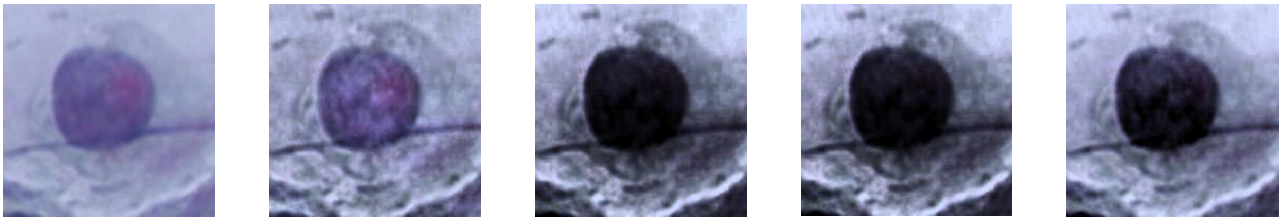

(a) Anisotropic Diffusion Filter | (b) CLAHE | (c) PAGCHE | (d) Histogram Equalisation | (e) Contrast Stretching

Fig. 6. Experimental results of Image 1 after applying Anisotropic Diffusion Filter followed by contrast enhancement methods (b-e)

(a) Bilateral Filter | (b) CLAHE | (c) PAGCHE | (d) Histogram Equalisation | (e) Contrast Stretching

Fig. 7. Experimental results of Image 1 after applying Bilateral Filter followed by contrast enhancement methods (b-e)

(a) Median Filter | (b) CLAHE | (c) PAGCHE | (d) Histogram Equalisation | (e) Contrast Stretching

Fig. 8. Experimental results of Image 1 after applying Median Filter followed by contrast enhancement methods (b-e)

(a) NLH Filter | (b) CLAHE | (c) PAGCHE | (d) Histogram Equalisation | (e) Contrast Stretching

Fig. 9. Experimental results of Image 1 after applying NLH Filter followed by contrast enhancement methods (b-e)

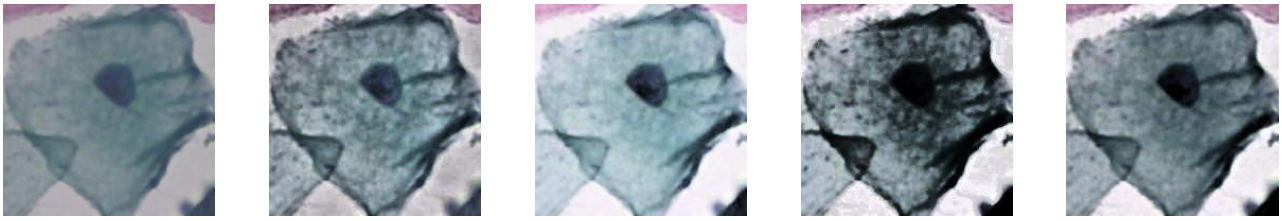

(a) Anisotropic Diffusion Filter (b) CLAHE (c) PAGCHE (d) Histogram Equalisation (e) Contrast Stretching

Fig. 10. Experimental results of Image 2 after applying Anisotropic Diffusion Filter followed by contrast enhancement methods (b-e)

(a) Bilateral Filter (b) CLAHE (c) PAGCHE (d) Histogram Equalisation (e) Contrast Stretching

Fig. 11. Experimental results of Image 2 after applying Bilateral Filter followed by contrast enhancement methods (b-e)

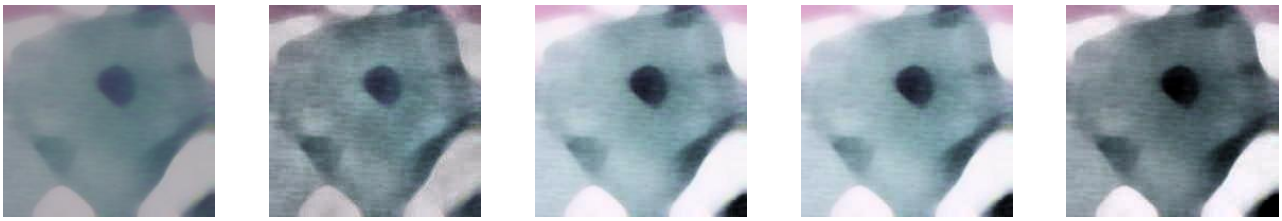

(a) Median Filter (b) CLAHE (c) PAGCHE (d) Histogram Equalisation (e) Contrast Stretching

Fig. 12. Experimental results of Image 2 after applying Median Filter followed by contrast enhancement methods (b-e)

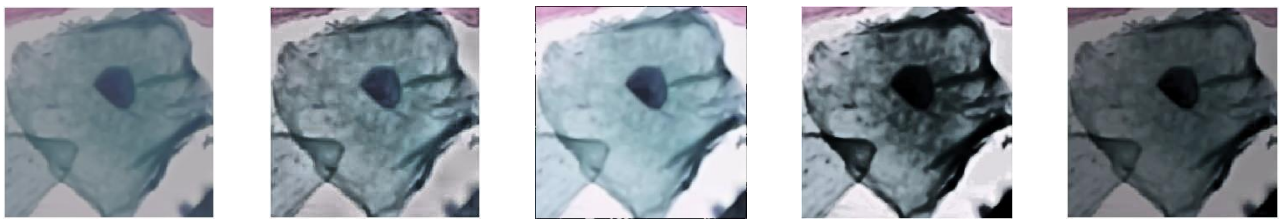

(a) NLH Filter (b) CLAHE (c) PAGCHE (d) Histogram Equalisation (e) Contrast Stretching

Fig. 13. Experimental results of Image 2 after applying NLH Filter followed by contrast enhancement methods (b-e)

(a) Anisotropic Diffusion Filter (b) CLAHE (c) PAGCHE (d) Histogram Equalisation (e) Contrast Stretching

Fig. 14. Experimental results of Image 3 after applying Anisotropic Diffusion Filter followed by contrast enhancement methods (b-e)

(a) Bilateral Filter (b) CLAHE (c) PAGCHE (d) Histogram Equalisation (e) Contrast Stretching

Fig. 15. Experimental results of Image 3 after applying Bilateral Filter followed by contrast enhancement methods (b-e)

(a) Median Filter (b) CLAHE (c) PAGCHE (d) Histogram Equalisation (e) Contrast Stretching

Fig. 16. Experimental results of Image 3 after applying Median Filter followed by contrast enhancement methods (b-e)

(a) NLH Filter (b) CLAHE (c) PAGCHE (d) Histogram Equalisation (e) Contrast Stretching

Fig. 17. Experimental results of Image 3 after applying NLH Filter followed by contrast enhancement methods (b-e)

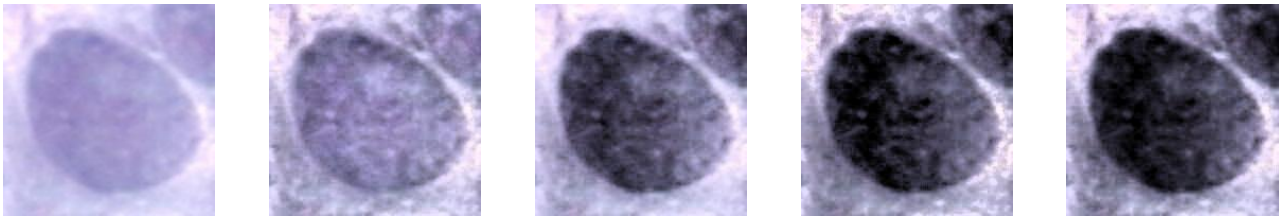

(a) Anisotropic Diffusion Filter (b) CLAHE (c) PAGCHE (d) Histogram Equalisation (e) Contrast Stretching

Fig. 18. Experimental results of Image 4 after applying Anisotropic Diffusion Filter followed by contrast enhancement methods (b-e)

(a) Bilateral Filter (b) CLAHE (c) PAGCHE (d) Histogram Equalisation (e) Contrast Stretching

Fig. 19. Experimental results of Image 4 after applying Bilateral Filter followed by contrast enhancement methods (b-e)

(a) Median Filter (b) CLAHE (c) PAGCHE (d) Histogram Equalisation (e) Contrast Stretching

Fig. 20. Experimental results of Image 4 after applying Median Filter followed by contrast enhancement methods (b-e)

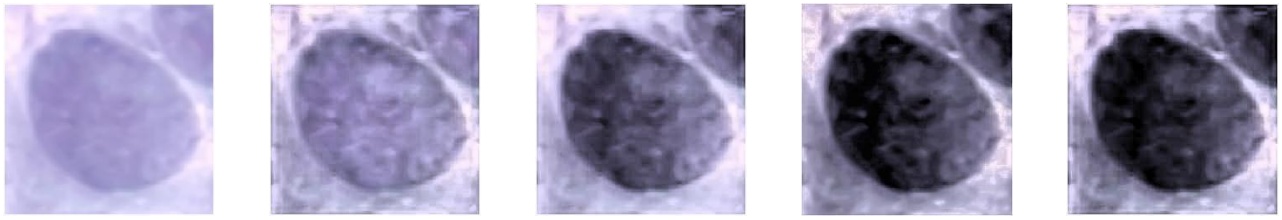

(a) NLH Filter (b) CLAHE (c) PAGCHE (d) Histogram Equalisation (e) Contrast Stretching

Fig. 21. Experimental results of Image 4 after applying NLH Filter followed by contrast enhancement methods (b-e)

3.2 Quantitative Analysis

Quantitative analysis is a mathematical process of gaining insight into the performance of an algorithm that does not require any human interaction. The nucleus and cytoplasm are in the foreground of smear photos, which have a lot of debris in the background. To overcome the limitation of visual experiments, statistical analysis tools, which rely on objective criteria and benchmark measurements, are used. Mean value (MV), standard deviation (STD) for contrast, structural

similarity index metric (SSIM), peak signal-to-noise ratio (PSNR), absolute mean brightness error (AMBE), and entropy are the measurement methods used in this work. The mathematical representation is shown in Eq. (10) to (15) below.

The mean value represents the average intensity of the image. It provides information about the overall brightness of the image. Larger mean values indicate brighter images, while smaller mean values indicate darker images.

$$Mean = \frac{1}{X \times Y} \sum_{x,y=0}^{x,y=X-1,Y-1} I(x,y), \tag{10}$$

where I(x, y) denotes the value at x and y points, and X and Y denote the size of image I.

STD measures the variation in intensity values, which correlates with visual contrast. Higher STD values indicate higher visual contrast and potentially more information.

$$STD = \sqrt{\frac{\sum_{x,y=0}^{x,y=X-1,Y-1} I(x,y) - (I(x,y) - Mean)}{X \times Y}} \tag{11}$$

where I(x, y) denotes the value at x and y points, and X and Y denote the size of image I and is $Mean$ the average intensity value of the image.

AMBE measures the difference in brightness between the original and processed images. Lower AMBE values indicate that the processed image's brightness is closer to the original.

$$AMBE = |Original_{Mean} - Processed_{Mean}| \tag{12}$$

where $Original_{Mean}$ is the mean intensity value of the original image and $Processed_{Mean}$ is the mean intensity value of the processed image.

SSIM is widely used to evaluate image quality since it imitates the human vision perspective of image structure. SSIM compares the luminance, contrast, and structure of original and processed images to determine the correlations between pixels. A value closer to one indicates that the two images are more similar and can be seen in Eq. (13):

$$SSIM(x,y) = \frac{(2\mu_x\mu_y + c_1)(2\sigma_{xy} + c_2)}{(\mu_x^2 + \mu_y^2 + c_1)(\sigma_x^2 + \sigma_y^2 + c_2)}, \tag{13}$$

where μ_x, μ_y are the means of x and y, respectively. σ_x^2, σ_y^2 are the variances of x and y, respectively, and σ_{xy} is the covariance of x and y.

The PSNR evaluates the ratio between the maximum possible power of a signal and the power of corrupting noise. Higher PSNR values indicate better image quality. The Eq. (14) is referred to.

$$PSNR = 10 \log_{10}\left(\frac{255^2}{MSE}\right) \tag{14}$$

Where $\log_{10}$ is the base-10 logarithm, 255 is the maximum possible pixel value of the image (for 8-bit images) and *MSE* is the Mean Squared Error between the original image and the processed image.

Entropy is a measure of the amount of information in images used to evaluate image quality. A higher value indicates that there are more details in an image. Entropy formula is as in Eq. (15):

$$Entropy = \sum_{V=0}^{V=255} p(V) \log_2 p(V), \quad (15)$$

where $p(V)$ is the probability of the grey value V in the image.

Each measurement technique's individual results are not significant on their own. High brightness levels, for example, are indicated by high mean and AMBE values. On the other hand, if the STD, SSIM, or PSNR values are low, this could result in missing data in the processed image. A significant difference in entropy between the processed and original images suggests a significant impact, potentially resulting in unwanted details and excessive noise in the processed images. As a result, it is not advisable to analyse the output image quality using only the results of earlier measurements. To assess performance, all measurement values must be examined together and their interactions considered.

Quantitative analysis was conducted after applying denoise and contrast enhancement methods to the original images. Table 4 shows the results of the evaluation based on the denoise filter. The study found that the median and bilateral filters, on average, decreased the mean value of the original image from 129.13 to 126.11 and 124.25, respectively. Meanwhile, on average, the anisotropic diffusion filter and NLH increased the mean value of the output images. STDs of the output images, in general, improved, with the median filter having the highest value at 63.85, followed by the bilateral filter at 62.37. Anisotropic diffusion and NLH filters produced STD scores of 58.17 and 48.54, respectively. In terms of AMBE, all the filters increased the score, with the anisotropic diffusion filter having the highest score at 22.48, followed by the median filter at 19.44. NLH and bilateral filters produced AMBE scores of 18.36 and 16.44, respectively. The SSIM score shows that NLH has the highest value of 0.82, followed by both anisotropic diffusion and bilateral filters with 0.75, and the median filter with 0.71. However, the anisotropic diffusion filter gives the best PSNR score with 18.46, followed by the NLH filter with 17.83. Meanwhile, the median and bilateral filters provide the lowest PSNR scores, with 15.38 and 16.32, respectively. Lastly, the entropy score increased for all filters, with the anisotropic diffusion filter producing a score of 7.52, and the bilateral filter producing a score of 7.44. In comparison, the median and NLH filters produced scores of 7.30 and 7.05, respectively.

Table 4
Average result based on denoising filters

Method	Mean	STD	AMBE	SSIM	PSNR	Entropy
Median	126.11	63.85	19.44	0.71	15.38	7.30
Anisotropic diffusion	133.57	58.17	22.48	0.75	18.46	7.52
Bilateral	124.25	62.37	16.44	0.75	16.32	7.44
NLH	136.19	48.54	18.36	0.82	17.83	7.05
Original	129.13	31.23	0	1	100	6.47

Table 5 shows the results of the evaluation based on the contrast enhancement. The research found that histogram equalisation and contrast stretching reduce the mean value of the original image from 129.13 to 115.52 and 112.42, respectively. PAGCHE and CLAHE, on the other hand, increase the mean value of the output images to 148.07 and 144.12, respectively. Histogram equalisation produced the highest STD score of 72.17, followed by PAGCHE with 60.4, and contrast stretching and CLAHE produced STD scores of 59.71 and 40.65, respectively. In terms of AMBE, all of

the filters improved the scores, with PAGCHE scoring the highest at 21.96 and contrast stretching scoring the lowest at 19.75. Histogram equalisation and CLAHE produced AMBE scores of 17.6 and 17.41, respectively. CLAHE has the highest SSIM score of 0.86, followed by PAGCHE and contrast stretching with scores of 0.78 and 0.76, respectively. Histogram equalisation, on the other hand, has the lowest SSIM score of 0.63. CLAHE gives the best PSNR score of 20.15, followed by contrast stretching with 18.93. PAGCHE and histogram equalisation, on the other hand, produce the lowest PSNR scores of 14.78 and 14.13, respectively. Finally, the entropy score for all filters increased, with histogram equalisation producing a score of 7.50 and PAGCHE producing a score of 7.42. In comparison, contrast stretching and CLAHE produced scores of 7.18 and 7.21, respectively.

Table 5
Average result of based on contrast enhancement methods

Method	Mean	STD	AMBE	SSIM	PSNR	Entropy
PAGCHE	148.07	60.4	21.96	0.78	14.78	7.42
Histogram Equalisation	115.52	72.17	17.6	0.63	14.13	7.50
Contrast Stretching	112.44	59.712	19.75	0.76	18.93	7.18
CLAHE	144.12	40.65	17.41	0.86	20.15	7.21
Original	129.13	31.23	0	1	100	6.47

Based on the quantitative and visual analysis results, several key points can be highlighted. The best method of choice depends on the purpose of pre-processing. This study aims to select the best pre-processing method to apply in nucleus segmentation. Hence, the priority of pre-processing is to differentiate the nucleus from the background, which includes the cytoplasm, interstitial fluid, and debris. Next, the image should be smoothed and noise removed while preserving the edges of the nucleus.

Visually and statistically, the median and bilateral filters give good results compared to the NLH and anisotropic diffusion filters. Meanwhile, the NLH and anisotropic diffusion filters have successfully preserved the debris and detail. To prove this, the two stated filters produced the highest PSNR scores, 18.46 and 17.83, respectively, as shown in Table 2. In addition, the SSIM scores for the same filters were also the highest, with 0.82 and 0.75, respectively. However, in terms of nucleus detection, the details, such as debris and texture, will result in poor segmentation performance due to the presence of noise. Comparing the bilateral and median filters, the bilateral filter produces a better result in terms of edge preservation, with a PSNR score of 16.32 and an SSIM score of 0.75. The median filter can be seen to remove noise better than the anisotropic diffusion filter. Hence, the median filter is the best filter to apply for nucleus detection.

In terms of contrast enhancement, it can be visually observed that PAGCHE provides the best visual and statistical results. The best result means that the method is able to provide high contrast standard deviation and accurately differentiate between the nucleus, intracellular fluids, and interstitial fluid. It is crucial to note that Image 2 has three visible main regions, which are the nucleus, cytoplasm, and interstitial fluid, compared to other images, which have only two visible main regions, the nucleus and the background. Based on the results of Image 1 and Image 2 from Figures 2-9(d-e), histogram equalisation and contrast stretching do not accurately differentiate the nucleus and cytoplasm. This is possibly the main reason the mean score of histogram equalisation and contrast stretching has been dragged lower than the original, as shown in Table 2. However, Images 3 and 4 from Figures 10-17 (d-e) produce good contrast output except for Figure 13(e) using the contrast stretching method. This is why the two stated methods have good STD and AMBE scores. Meanwhile, the anisotropic diffusion filter produces poor performance compared to the others as it is unable to

improve the contrast of the low-contrast images, such as Images 3 and 4. In brief, PAGCHE produces the highest mean and AMBE scores, indicating good contrast enhancement while maintaining a relatively high value of STD. Visually, it is able to successfully differentiate between the interstitial fluid, the cytoplasm, and the nucleus for the four filters applied.

4. Conclusions

In this research, several methods for noise removal and contrast enhancement methods were analysed. There are two main stages: noise removal and contrast enhancement. Each stage will compare one state-of-arts method with the other three classical methods. This study used NLH for noise removal and PAGCHE for contrast enhancement. The original RGB images are transformed into the HSV colour space to maintain the colour, and the V channel is used for enhancement. The best combination methods must increase the contrast while significantly differentiating between the nucleus, cytoplasm, and interstitial fluid. The filter must be able to smoothen the noise texture and remove the debris while preserving the interested object's edges and colour details. Results show that the median filter produces the best result regarding smoothening and debris removal in visual analysis. The PAGCHE method produces the best brightness and contrast improvement results based on visual and quantitative analysis. Combining the Median Filter and PAGCHE methods may meet the stated characteristics by significantly removing noise and improving the colour image's low contrast and poor illumination while retaining the colour and required edges. Compared to other methods, it is the most flexible, regardless of the type of image used.

Acknowledgement

This research was supported by funding from the Ministry of Higher Education (MoHE) Malaysia under the Fundamental Research Grant Scheme (FRGS/1/2021/SKK0/UNIMAP/02/1).

References

[1] Ulasan, Suatu, N. A. D. Z. I. R. A. H. Nahrawi, W. A. Mustafa, and S. N. A. M. Kanafiah. "Knowledge of Human Papillomavirus (HPV) and cervical cancer among Malaysia Residents: A review." Sains Malaysiana 49, no. 7 (2020): 1687-95. https://doi.org/10.17576/jsm-2020-4907-19

[2] Sausen, Daniel G., Oren Shechter, Elisa S. Gallo, Harel Dahari, and Ronen Borenstein. "Herpes Simplex Virus, Human Papillomavirus, and Cervical Cancer: Overview, Relationship, and Treatment Implications." Cancers 15, no. 14 (2023): 3692. https://doi.org/10.3390/cancers15143692

[3] Guimarães, Yasmin Medeiros, Luani Rezende Godoy, Adhemar Longatto-Filho, and Ricardo dos Reis. "Management of early-stage cervical cancer: a literature review." Cancers 14, no. 3 (2022): 575. https://doi.org/10.3390/cancers14030575

[4] Sung, Hyuna, Jacques Ferlay, Rebecca L. Siegel, Mathieu Laversanne, Isabelle Soerjomataram, Ahmedin Jemal, and Freddie Bray. "Global cancer statistics 2020: GLOBOCAN estimates of incidence and mortality worldwide for 36 cancers in 185 countries." CA: a cancer journal for clinicians 71, no. 3 (2021): 209-249. https://doi.org/10.3322/caac.21660

[5] Mustafa, W. A., Halim, A., & Ab Rahman, K. S. (2020). A Narrative Review: Classification of Pap Smear Cell Image for Cervical Cancer Diagnosis. Oncologie (Tech Science Press), 22(2). https://doi.org/10.32604/oncologie.2020.013660

[6] Mustafa, Wan Azani, Low Zhe Wei, and Khairul Shakir Ab Rahman. "Automated Cell Nuclei Segmentation on Cervical Smear Images Using Structure Analysis." Journal of Biomimetics, Biomaterials and Biomedical Engineering 51 (2021): 105-115. https://doi.org/10.4028/www.scientific.net/JBBBE.51.105

[7] Mustafa, Wan Azani, Afiqah Halim, Mohd Aminudin Jamlos, and Syed Zulkarnain Syed Idrus. "A Review: Pap smear analysis based on image processing approach." In Journal of Physics: Conference Series, vol. 1529, no. 2, p. 022080. IOP Publishing, 2020. https://doi.org/10.1088/1742-6596/1529/2/022080

[8] Patel, Mandakini M., Amrish N. Pandya, and Jigna Modi. "Cervical Pap smear study and its utility in cancer screening, to specify the strategy for cervical cancer control." National journal of community medicine 2, no. 01 (2011): 49-51. https://doi.org/10.18203/2320-1770.ijrcog20213478

[9] Macios, Anna, and Andrzej Nowakowski. "False Negative Results in Cervical Cancer Screening—Risks, Reasons and Implications for Clinical Practice and Public Health." Diagnostics 12, no. 6 (2022): 1508. https://doi.org/10.3390/diagnostics12061508

[10] Schiffman, Mark, and Silvia de Sanjose. "False positive cervical HPV screening test results." Papillomavirus Research 7 (2019): 184-187. https://doi.org/10.1016/j.pvr.2019.04.012

[11] Hameed, Mohamed Saifuddin Shahul, Wan Azani Mustafa, Syed Zulkarnain Syed Idrus, Mohd Aminudin Jamlos, and Hiam Alquran. "Contrast enhancement on pap smear cell images: A comparison." In AIP Conference Proceedings, vol. 2608, no. 1. AIP Publishing, 2023. https://doi.org/10.1063/5.0127797

[12] Nahrawi, Nadzirah, Wan Azani Mustafa, Siti Nurul Aqmariah Mohd Kanafiah, and Mohd Yusoff Mashor. "Color Contrast Enhancement on Pap Smear Images Using Statistical Analysis." Intelligent Automation & Soft Computing 30, no. 2 (2021). https://doi.org/10.32604/iasc.2021.018635

[13] Nahrawi, Nadzirah, Wan Azani Mustafa, Siti Nurul Aqmariah Mohd Kanafiah, Mohd Aminudin Jamlos, and Wan Khairunizam. "Contrast enhancement approaches on medical microscopic images: a review." In Proceedings of the 11th National Technical Seminar on Unmanned System Technology 2019: NUSYS'19, pp. 715-726. Springer Singapore, 2021. https://doi.org/10.1007/978-981-15-5281-6_51

[14] Wang, Wencheng, Xiaojin Wu, Xiaohui Yuan, and Zairui Gao. "An experiment-based review of low-light image enhancement methods." Ieee Access 8 (2020): 87884-87917. https://doi.org/10.1109/ACCESS.2020.2992749

[15] Jian, Muwei, Xiangyu Liu, Hanjiang Luo, Xiangwei Lu, Hui Yu, and Junyu Dong. "Underwater image processing and analysis: A review." Signal Processing: Image Communication 91 (2021): 116088. https://doi.org/10.1016/j.image.2020.116088

[16] Bataineh, Bilal. "Brightness and Contrast Enhancement Method for Color Images via Pairing Adaptive Gamma Correction and Histogram Equalization." Available at SSRN 4044239 (2023). https://doi.org/10.2139/ssrn.4044239

[17] Mustafa, Wan Azani, and Mohamed Mydin M. Abdul Kader. "Contrast enhancement based on fusion method: a review." In Journal of Physics: Conference Series, vol. 1019, no. 1, p. 012025. IOP Publishing, 2018. https://doi.org/10.1088/1742-6596/1019/1/012025

[18] Dhal, Krishna Gopal, Arunita Das, Swarnajit Ray, Jorge Gálvez, and Sanjoy Das. "Histogram equalization variants as optimization problems: a review." Archives of Computational Methods in Engineering 28 (2021): 1471-1496. https://doi.org/10.1007/s11831-020-09425-1

[19] Maurya, Lalit, Viney Lohchab, Prasant Kumar Mahapatra, and János Abonyi. "Contrast and brightness balance in image enhancement using Cuckoo Search-optimized image fusion." Journal of King Saud University-Computer and Information Sciences 34, no. 9 (2022): 7247-7258. https://doi.org/10.1016/j.jksuci.2021.07.008

[20] Huang, Thomas, G. J. T. G. Y. Yang, and Greory Tang. "A fast two-dimensional median filtering algorithm." IEEE transactions on acoustics, speech, and signal processing 27, no. 1 (1979): 13-18. https://doi.org/10.1109/TASSP.1979.1163188

[21] Hunt, B. R. "Computer vision: a first course: D Boyle and RC Thomas. Published by Blackwell Scientific Publications, UK. 1988. 210pp£ 12.95." (1990): 171. https://doi.org/10.1016/0262-8856(90)90039-8

[22] Ziegel, Eric R. "Filtering in the Time and Frequency Domains." (1988): 245-245. https://doi.org/10.1080/00401706.1988.10488394

[23] Starck, Jean-Luc, Emmanuel J. Candès, and David L. Donoho. "The curvelet transform for image denoising." IEEE Transactions on image processing 11, no. 6 (2002): 670-684. https://doi.org/10.1109/TIP.2002.1014998

[24] Buades, Antoni, Bartomeu Coll, and J-M. Morel. "A non-local algorithm for image denoising." In 2005 IEEE computer society conference on computer vision and pattern recognition (CVPR'05), vol. 2, pp. 60-65. Ieee, 2005. https://doi.org/10.1109/CVPR.2005.38

[25] Sheela, C. Jaspin Jeba, and G. Suganthi. "An efficient denoising of impulse noise from MRI using adaptive switching modified decision based unsymmetric trimmed median filter." Biomedical Signal Processing and Control 55 (2020): 101657. https://doi.org/10.1016/j.bspc.2019.101657

[26] Goyal, Bhawna, Ayush Dogra, Dawa Chyophel Lepcha, Deepika Koundal, Adi Alhudhaif, Fayadh Alenezi, and Sara A. Althubiti. "Multi-modality image fusion for medical assistive technology management based on hybrid domain filtering." Expert Systems with Applications 209 (2022): 118283. https://doi.org/10.1016/j.eswa.2022.118283

[27] Göreke, Volkan. "A novel method based on Wiener filter for denoising Poisson noise from medical X-Ray images." Biomedical Signal Processing and Control 79 (2023): 104031. https://doi.org/10.1016/j.bspc.2022.104031

[28] Gautam, Divya, Kavita Khare, and Bhavana P. Shrivastava. "A Novel Guided Box Filter Based on Hybrid Optimization for Medical Image Denoising." Applied Sciences 13, no. 12 (2023): 7032. https://doi.org/10.3390/app13127032

[29] Ghumaan, Rajanbir Singh, Prateek Jeet Singh Sohi, Nikhil Sharma, and Bharat Garg. "A novel hybrid decision-based filter and universal edge-based logical smoothingadd-on to remove impulsive noise." Turkish Journal of Electrical Engineering and Computer Sciences 29, no. 4 (2021): 1944-1963. https://doi.org/10.3906/elk-2005-12
[30] Sharma, Nikhil, Prateek Jeet Singh Sohi, and Bharat Garg. "An adaptive weighted min-mid-max value based filter for eliminating high density impulsive noise." Wireless Personal Communications 119 (2021): 1975-1992. https://doi.org/10.1007/s11277-021-08314-5
[31] Suhaili, Shamsiah, Joyce Shing Yii Huong, Asrani Lit, Kuryati Kipli, Maimun Huja Husin, Mohamad Faizrizwan Mohd Sabri, and Norhuzaimin Julai. 2024. "Development of Digital Image Processing Algorithms via FPGA Implementation". Semarak International Journal of Electronic System Engineering 3 (1):28-45. https://doi.org/10.37934/sijese.3.1.2845
[32] Qi, Yunliang, Zhen Yang, Wenhao Sun, Meng Lou, Jing Lian, Wenwei Zhao, Xiangyu Deng, and Yide Ma. "A comprehensive overview of image enhancement techniques." Archives of Computational Methods in Engineering (2021): 1-25. https://doi.org/10.1007/s11831-021-09587-6
[33] Bala, A.Anilet, Pranav Pranshu, Kanwar, Shipra Das and Debottam Das. "Retinal Image Enhancement Based on Contrast, Luminosity Adjustment and MSC." International Journal of Recent Technology and Engineering (2019): n. pag. https://doi.org/10.35940/ijrte.b1306.0982s1119
[34] Al-Amri, Salem Saleh, N. V. Kalyankar, and S. D. Khamitkar. "Linear and non-linear contrast enhancement image." IJCSNS International Journal of Computer Science and Network Security 10, no. 2 (2010): 139-143. https://doi.org/10.48550/arXiv.1005.4020
[35] Zhou, Mei, Kai Jin, Shaoze Wang, Juan Ye, and Dahong Qian. "Color retinal image enhancement based on luminosity and contrast adjustment." IEEE Transactions on Biomedical engineering 65, no. 3 (2017): 521-527. https://doi.org/10.1109/TBME.2017.2700627
[36] Rao, Karishma, Manu Bansal, and Gagandeep Kaur. "A hybrid method for improving the luminosity and contrast of color retinal images using the JND model and multiple layers of CLAHE." Signal, Image and Video Processing 17, no. 1 (2023): 207-217. https://doi.org/10.1007/s11760-022-02223-1
[37] Saroj, Sushil Kumar. "An efficient hybrid approach for medical images enhancement." ELCVIA Electronic Letters on Computer Vision and Image Analysis 21, no. 2 (2022): 62-76. https://doi.org/10.5565/rev/elcvia.1574
[38] Mousania, Younes, Salman Karimi, and Ali Farmani. "Optical remote sensing, brightness preserving and contrast enhancement of medical images using histogram equalization with minimum cross-entropy-Otsu algorithm." Optical and Quantum Electronics 55, no. 2 (2023): 105. https://doi.org/10.1007/s11082-022-04341-z
[39] J. W. Tukey, "Exploratory Data Analysis by John W. Tukey," Biometrics, vol. 33. 1977.
[40] Paris, Sylvain, Pierre Kornprobst, Jack Tumblin, and Frédo Durand. "Bilateral filtering: Theory and applications." Foundations and Trends® in Computer Graphics and Vision 4, no. 1 (2009): 1-73. https://doi.org/10.1561/0600000020
[41] Hou, Yingkun, Jun Xu, Mingxia Liu, Guanghai Liu, Li Liu, Fan Zhu, and Ling Shao. "NLH: A blind pixel-level non-local method for real-world image denoising." IEEE Transactions on Image Processing 29 (2020): 5121-5135. https://doi.org/10.1109/TIP.2020.2980116
[42] Poynton, Charles. Digital video and HD: Algorithms and Interfaces. Elsevier, 2012. https://doi.org/10.1016/B978-0-12-391926-7.50063-1
[43] Muhammad Nazim, Nor' Awatif Amri, Normi Abdul Hadi, Mohd Rijal Ilias, Dian Kurniasari, and Suhaila Abd Halim. 2024. "Application of Different Distance Metrics on K-Means Clustering Algorithm for Retinal Vessel Images". Semarak International Journal of Machine Learning 4 (1):14-26. https://doi.org/10.37934/sijml.4.1.1426
[44] Dzulkifli, Fahmi Akmal. "Identification of Suitable Contrast Enhancement Technique for Improving the Quality of Astrocytoma Histopathological Images." ELCVIA Electronic Letters on Computer Vision and Image Analysis 20, no. 1 (2021): 84-98. http://dx.doi.org/10.5565/rev/elcvia.1256
[45] Lucknavalai, Karen, and Jürgen P. Schulze. "Real-time contrast enhancement for 3D medical images using histogram equalization." In Advances in Visual Computing: 15th International Symposium, ISVC 2020, San Diego, CA, USA, October 5–7, 2020, Proceedings, Part I 15, pp. 224-235. Springer International Publishing, 2020. https://dx.doi.org/10.1007/978-3-030-64556-4_18
[46] SM, PIZER. "Adaptive histogram equalization and its variations." Computer Graphics and Image Processing 6 (1977): 184-195. https://doi.org/10.1016/S0146-664X(77)80011-7
[47] Gonzalez, Rafael C. Digital image processing. Pearson education India, 2009. https://doi.org/10.1117/1.3115362